Nanoscale

SUPPLEMENTARY INFORMATION

Moiré Patterns of Twisted Bilayer Antimonene and their Structural and Electronic Transition

Qi An,[*a,b] **Oussama Moutanabbir ,**[b] **and Hong Guo**[a]

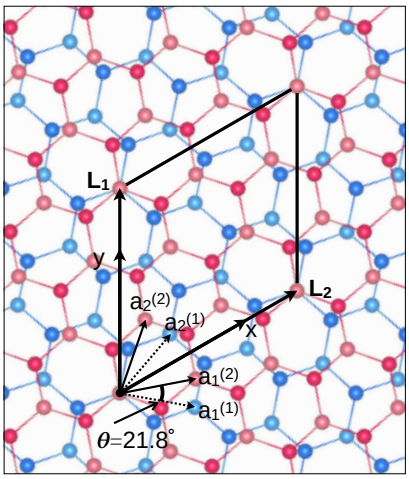

Fig. S1 Twisted bilayer antimonene originated from the AA high-symmetry stacking at the rotation angle $\theta = 21.8°$. The light blue and navy blue balls represent atoms of two sub-layers in the bottom layer of antimonene. The light and dark pink balls represent atoms of two sub-layers in the top layer of antimonene. $\vec{\mathbf{L}}_1$ and $\vec{\mathbf{L}}_2$ are the lattice vectors of the moiré superlattice (MSL). $(\vec{\mathbf{a}}_1^{(1)}, \vec{\mathbf{a}}_2^{(1)})$ and $(\vec{\mathbf{a}}_1^{(2)}, \vec{\mathbf{a}}_2^{(2)})$ are the lattice vectors of the bottom and top layer, respectively.

For commensurate bilayers, i.e. the case of the high-symmetry stackings of bilayer antimonene, we define the lattice vectors of the moiré superlattice $\vec{\mathbf{L}}_1$ and $\vec{\mathbf{L}}_2$ as the least common multiples of the unit cell vectors of the two layers. $\vec{\mathbf{L}}_2$ is obtained by rotating $\vec{\mathbf{L}}_1$ by 60°. $\vec{\mathbf{L}}_1$ is given by integers m, n, m', n' as

$$\vec{\mathbf{L}}_1 = m\vec{\mathbf{a}}_1^{(1)} + n\vec{\mathbf{a}}_2^{(1)} = m'\vec{\mathbf{a}}_1^{(2)} + n'\vec{\mathbf{a}}_2^{(2)} \tag{1}$$

where $(\vec{\mathbf{a}}_1^{(1)}, \vec{\mathbf{a}}_2^{(1)})$ and $(\vec{\mathbf{a}}_1^{(2)}, \vec{\mathbf{a}}_2^{(2)})$ are the lattice vectors of the bottom and top layer, respectively. DFT calculation is done on super-cells of moiré superlattice with periodicity. At certain angle θ, where the indices (m', n') is equal to (m, n), the superlattice becomes rigorously periodic. The rotation angle θ is then given by

[a] *Department of Physics, McGill University, 3600 rue university, Montréal, Québec, H3A 2T8, Canada. Email: qi.an@mail.mcgill.ca*
[b] *Department of Engineering Physics, École Polytechnique de Montréal, C. P. 6079, Succursale Centre-Ville, Montréal, Québec, H3C 3A7, Canada.*

$$\cos\theta = \frac{1}{2}\frac{m^2+n^2+4mn}{m^2+n^2+mn} \tag{2}$$

and the the moiré lattice constant can be written as

$$L = |\vec{\mathbf{L}}_1| = |\vec{\mathbf{L}}_2| = a\sqrt{m^2+n^2+mn} = \frac{|m-n|}{2\sin(\theta/2)}a \tag{3}$$

where a = $|\vec{\mathbf{a}}_1|$ = $|\vec{\mathbf{a}}_2|$ is the lattice constant of bilayer antimonene with AA or AB stackings.

Table S1 The structural information and formation energy E_{for} of twisted bilayer antimonene originated from AA and AB high-symmetry stackings at different rotation angles θ.

(m, n)	θ (°)	$L_{AA-\theta}$ (Å)	$E_{for_{AA-\theta}}$ (meV)	$L_{AB-\theta}$ (Å)	$E_{for_{AB-\theta}}$ (meV)	N
(1, 2)	21.80	10.84	67.51	11.15	45.94	28
(2, 3)	13.17	17.87	42.15	18.37	46.35	76
(3, 4)	9.43	24.93	45.81	25.63	46.71	148
(4, 5)	7.34	31.83	44.16	32.91	48.30	244
(5, 6)	6.01	38.88	46.97	40.20	51.88	364
(6, 7)	5.09	45.93	42.44	47.49	43.91	508
(7, 8)	4.41	52.98	41.14	54.78	40.20	676
(8, 9)	3.89	60.38	39.32	62.07	34.95	868

$L_{AA-\theta}$: Lattice constant of AA-θ MSL.

$L_{AB-\theta}$: Lattice constant of AB-θ MSL.

N: The number of atoms in each MSL.

Using the calculated electronic band structure $E(\mathbf{k})$ where $\mathbf{k}$ is the wave vector, the carrier effective mass m^* can be numerically determined by fitting to the second derivative of $E(\mathbf{k})$ at the band minimum (for electrons) or maximum (for holes):

$$m^{*^{-1}} = \frac{1}{\hbar}\frac{\partial^2}{\partial k^2}E(k) \tag{4}$$

where $\hbar$ is the reduced Planck constant. For the rather flat band at VBM, m^* is rather large: several times larger than the bare mass m_0 ($m^* > 2m_0$). For the dispersive bands at CBM, the fitted m^* is listed in Table S2.

Table S2 The calculated values of the effective mass m_e^* of CBM in units of bare mass m_0.

θ (°)	AA-θ m_e^*	AB-θ m_e^*	
		Γ-K	Γ-M
6.01	0.35	0.18	0.19
5.09	0.34	0.08	0.07
4.41	0.19	0.10	0.05
3.89	0.26	0.18	0.07

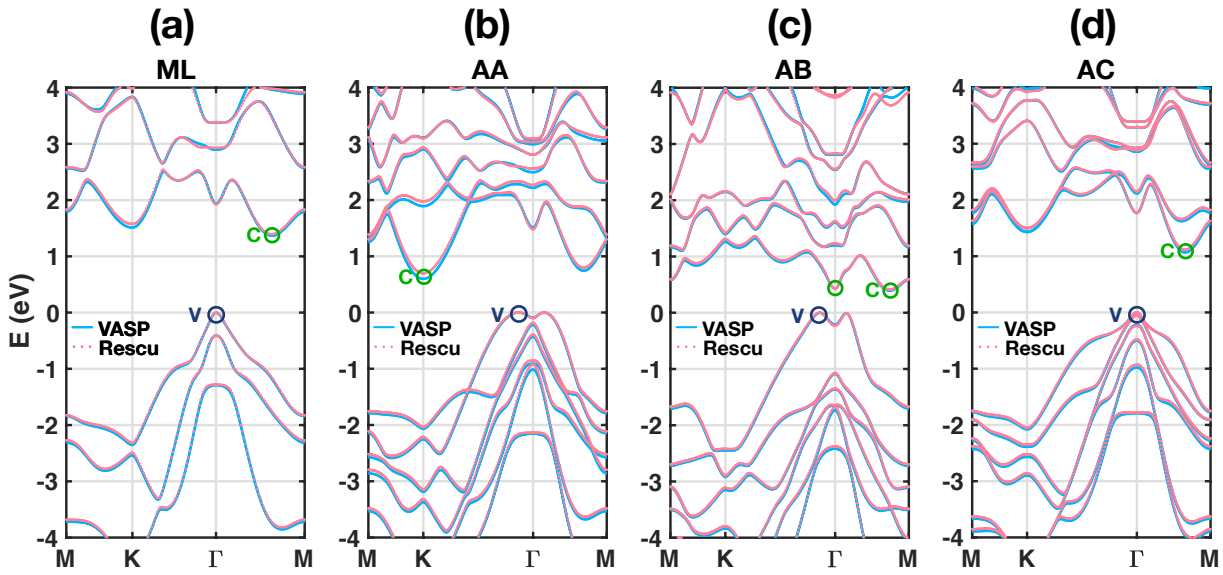

Fig. S2 Band structures of the (a) monolayer antimonene, (b)isolated bilayer antimonene with AA high-symmetry stacking, (c) isolated bilayer antimonene with AB high-symmetry stacking, (d) isolated bilayer antimonene with AC high-symmetry stacking calculated with HSE06 functional including SOC by VASP (blue solid lines) and RESCU (pink dotted lines) using optimized triple-zeta polarized (TZP) atomic orbital basis set. The VBM is shifted to zero to make a comparison between results from VASP and RESCU.

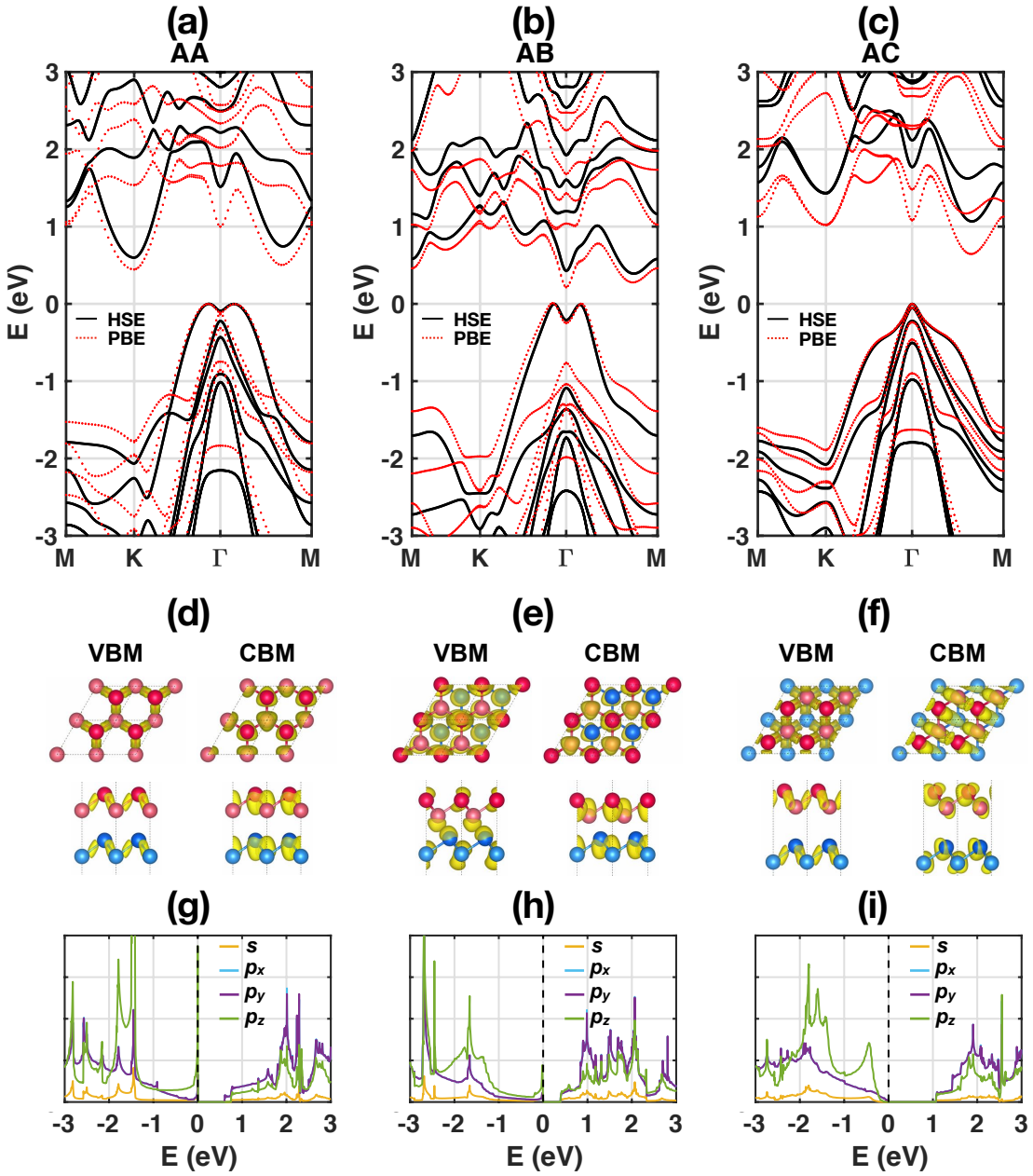

Fig. S3 Band structures of the (a) AA, (b) AB and (c) AC high symmetry stacking calculated with HSE06 functional including SOC (black solid lines) and PBE functional including SOC (red dashed lines), respectively. The VBM is shifted to zero to make a comparison between results from HSE06 and PBE functional. Top view and side view of the spatial distribution of wave functions $|\psi|^2$ at VBM and CBM of (d) AA, (e) AB and (f) AC high symmetry stacking. An uniform increment is used. Partial density of states (PDOS) on the *s* and *p* orbital of the (g) AA, (h) AB and (i) AC high symmetry stacking.

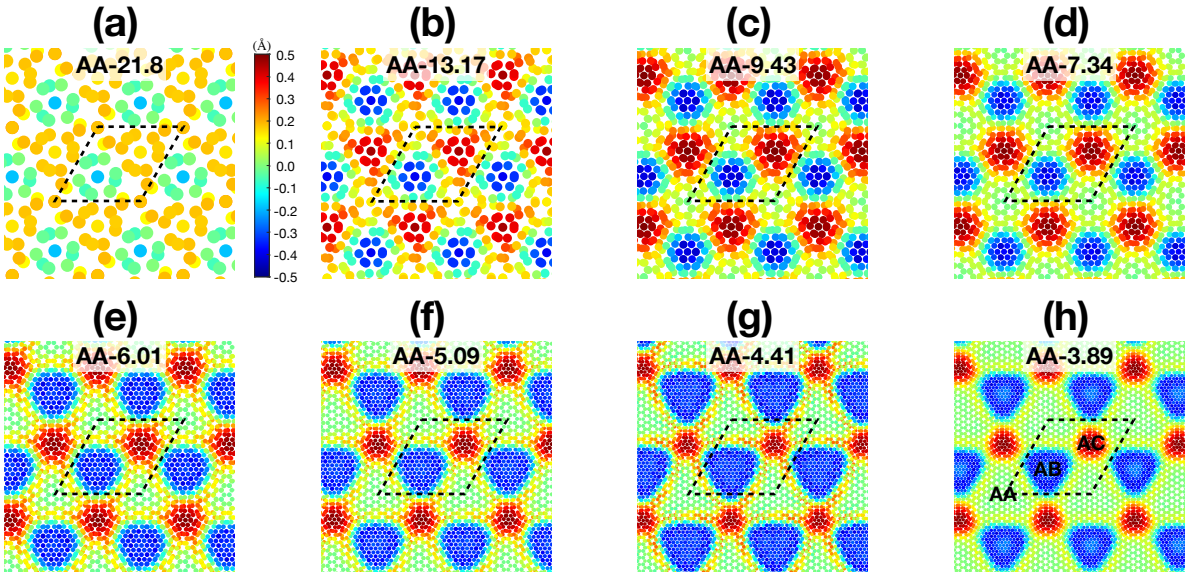

Fig. S4 The distribution of the out-of-plane displacement vector $\vec{o}$ in the relaxed AA-θ moiré superlattice. (a)-(h) correspond to $\theta = 21.8°$, $13.17°$, $9.43°$, $7.34°$, $6.01°$, $5.09°$, $4.41°$ and $3.89°$, respectively. The color map shows the values of $\vec{o}$. The unit cell of the moiré superlattice is marked by black dash lines and the marked high-symmetry stacking regions are given in (h) as an example.

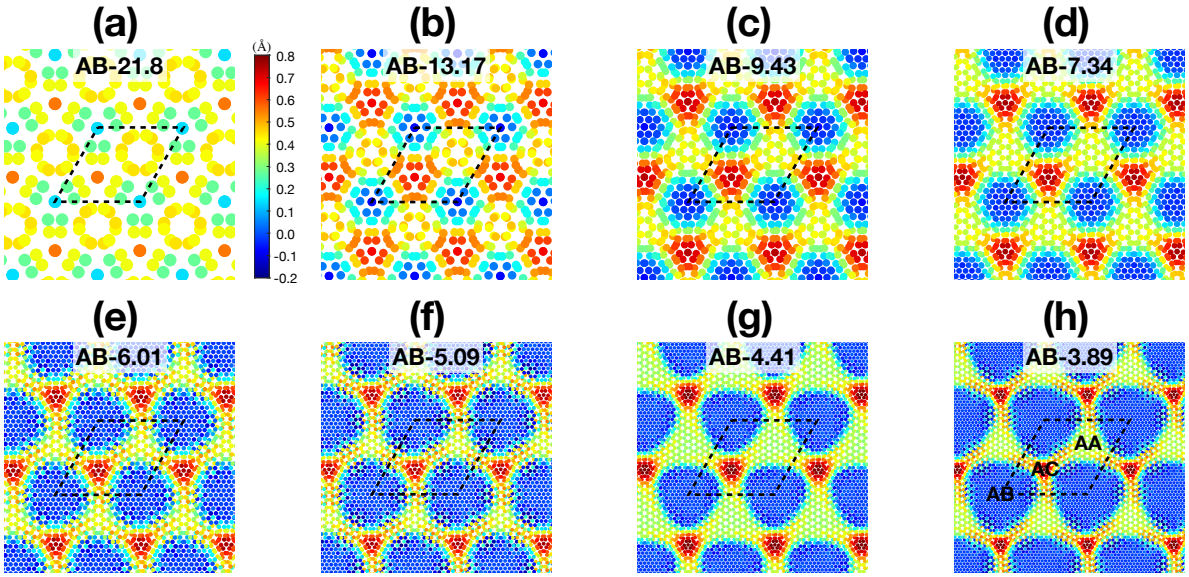

Fig. S5 The distribution of the out-of-plane displacement vector $\vec{o}$ in the relaxed AB-θ moiré superlattice. (a)-(h) correspond to $\theta = 21.8°$, $13.17°$, $9.43°$, $7.34°$, $6.01°$, $5.09°$, $4.41°$ and $3.89°$, respectively. The color map shows the values of $\vec{o}$. The unit cell of the moiré superlattice is marked by black dash lines and the marked high-symmetry stacking regions are given in (h) as an example.

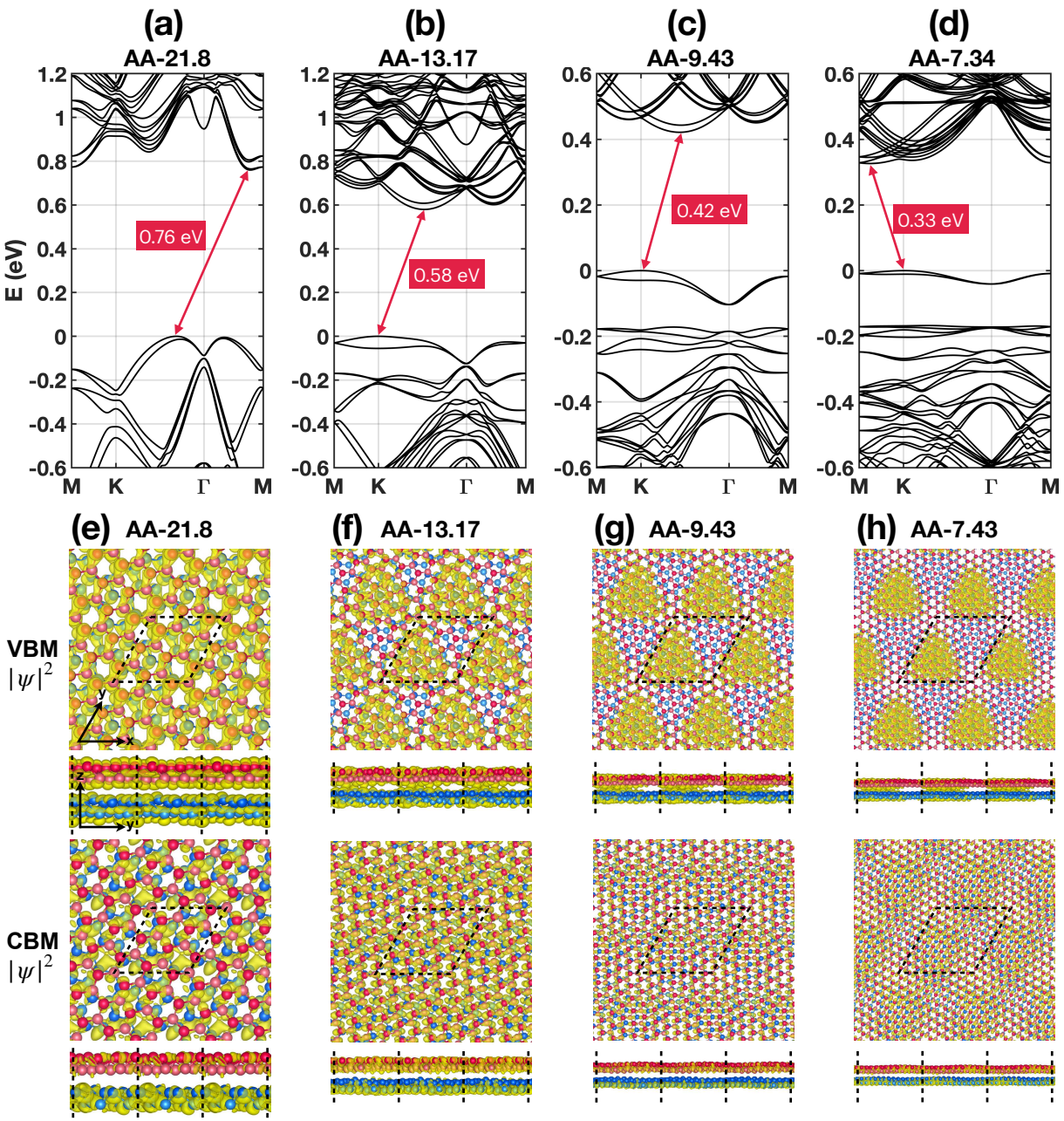

Fig. S6 Electronic band structure of the relaxed (a) AA-21.8, (b) AA-13.17, (c) AA-9.43 and (d) AA-7.34 MSL in the vicinity of the Fermi level calculated with PBE functional including SOC. The VBM is shifted to zero and the band gap is also given. Top view and side view of the spatial distribution of wave functions $|\psi|^2$ at VBM and CBM of the relaxed (e) AA-21.8, (f) AA-13.17, (g) AA-9.43 and (h) AA-7.34 MSL. An uniform increment is used.

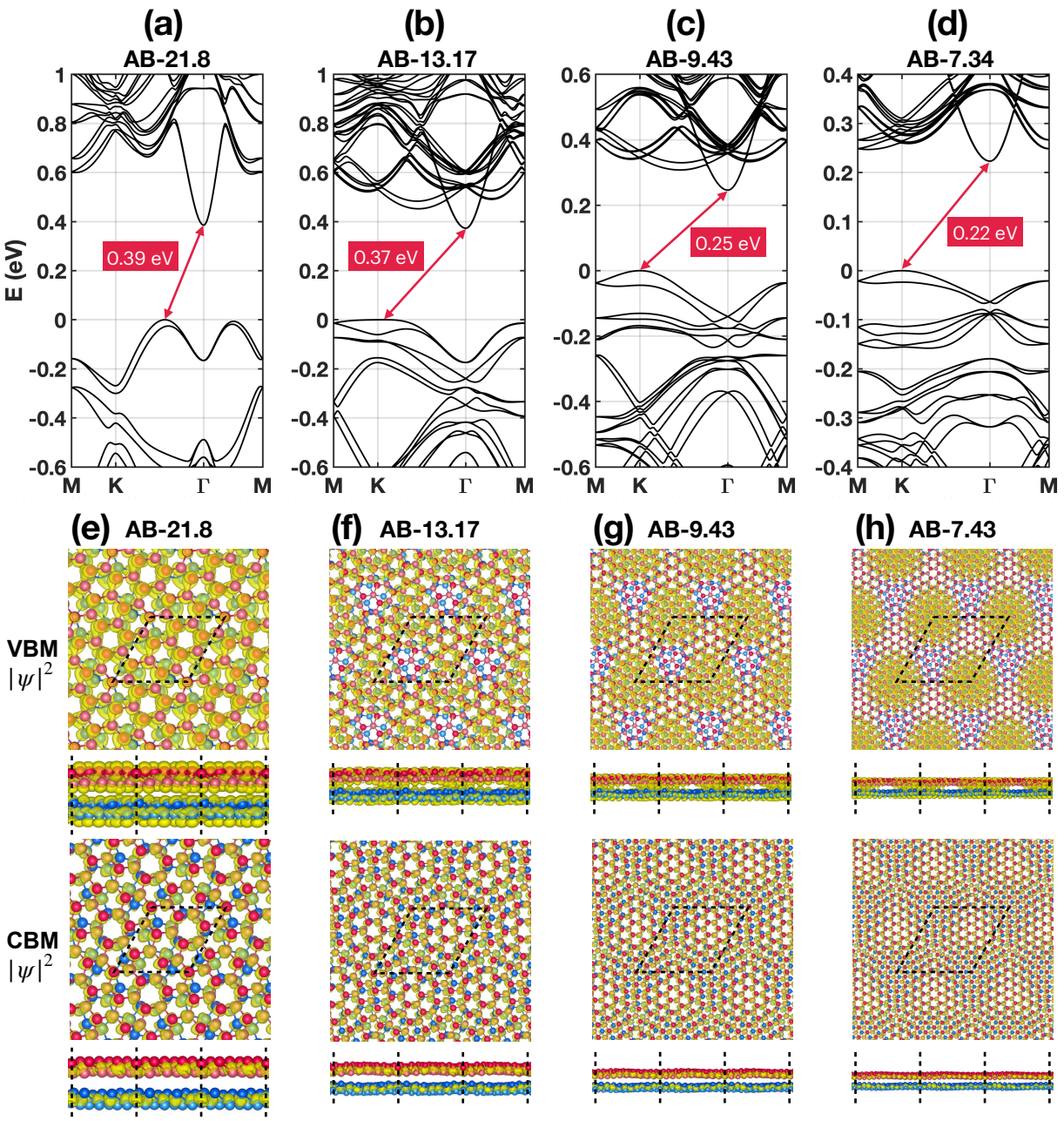

Fig. S7 Electronic band structure of the relaxed (a) AB-21.8, (b) AB-13.17, (c) AB-9.43 and (d) AB-7.34 MSL in the vicinity of the Fermi level calculated with PBE functional including SOC. The VBM is shifted to zero and the band gap is also given. Top view and side view of the spatial distribution of wave functions $|\psi|^2$ at VBM and CBM of the relaxed (e) AB-21.8, (f) AB-13.17, (g) AB-9.43 and (h) AB-7.34 MSL. An uniform increment is used.

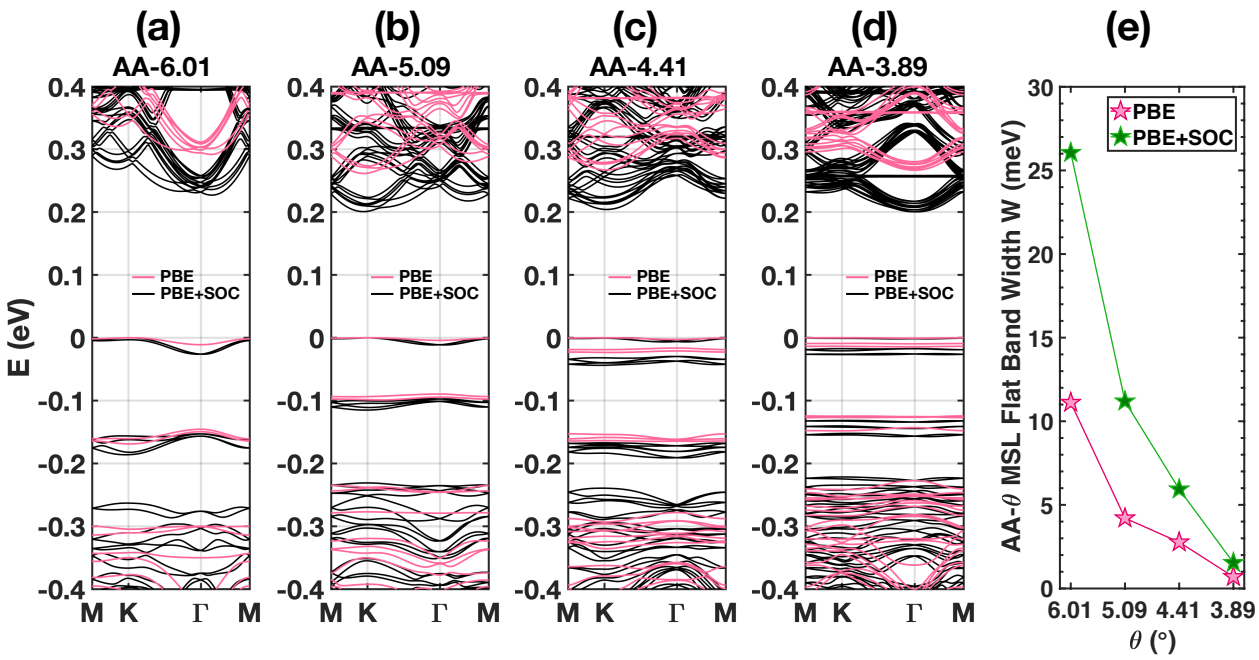

Fig. S8 Electronic band structure of (a) AA-6.01, (b) AA-5.09, (c) AA-4.41 and (d) AA-3.89 MSL calculated with PBE functional with SOC (black lines) and without SOC (pink lines) respectively. The VBM is shifted to zero. (e) Variations of the flat band width W with rotation angle θ for AA-θ MSL calculated with and without SOC. The green line with star markers corresponds to PBE with SOC and the pink line with star markers corresponds to PBE without SOC. The flat band width W is defined as the difference between the maximum and minimum energy in the top valance band.